North Atlantic Climate Response to Lake Agassiz Drainage at Coarse and Ocean Eddy-Permitting Resolutions

PAUL SPENCE

Climate Change Research Centre, University of New South Wales, Sydney, New South Wales, Australia

OLEG A. SAENKO

Canadian Centre for Climate Modelling and Analysis, Environment Canada, Victoria, British Columbia, Canada

WILLEM SIJP AND MATTHEW H. ENGLAND

Climate Change Research Centre, University of New South Wales, Sydney, New South Wales, Australia

(Manuscript received 16 November 2011, in final form 2 October 2012)

ABSTRACT

The North Atlantic climate response to the catastrophic drainage of proglacial Lake Agassiz into the Labrador Sea is analyzed with coarse and ocean eddy-permitting versions of a global coupled climate model. The North Atlantic climate response is qualitatively consistent in that a large-scale cooling is simulated regardless of the model resolution or region of freshwater discharge. However, the magnitude and duration of the North Atlantic climate response is found to be sensitive to model resolution and the location of freshwater forcing. In particular, the long-term entrainment of freshwater along the boundary at higher resolution and its gradual, partially eddy-driven escape into the interior leads to low-salinity anomalies persisting in the subpolar Atlantic for decades longer. As a result, the maximum decline of the Atlantic meridional overturning circulation (AMOC) and the ocean meridional heat transport (MHT) is amplified by about a factor of 2 at ocean eddy-permitting resolution, and the recovery is delayed relative to the coarse grid model. This, in turn, increases the long-term cooling in the high-resolution simulations. A decomposition of the MHT response reveals an increased role for transients and the horizontal mean component of MHT at higher resolution. With fixed wind stress curl, it is a stronger response of bottom pressure torque to the freshwater forcing at higher resolution that leads to a larger anomaly of the depth-integrated circulation.

1. Introduction

Computational constraints have limited the vast majority of centennial-time-scale global climate simulations to coarse horizontal resolutions (i.e., $>1°$) capable of resolving only large-scale ocean circulation features. Given that most of the observed ocean kinetic energy occurs on the mesoscale, with length scales from 10 to 100 km (Ducet et al. 2000; Wunsch 2007), these simulations are heavily reliant on parameterization schemes to account for unresolved flows. The Intergovernmental Panel on Climate Change (IPCC) Third Assessment Report notes considerable debate regarding the adequacy of coarse-resolution ocean models (McAvaney et al. 2001), and the Fourth Assessment Report further identifies the lack of a comprehensive suite of high-resolution global climate integrations as restricting the ability to draw firm conclusions (Randall et al. 2007). Unfortunately, computational constraints currently limit ocean mesoscale resolving simulations to nonglobal spatial domains with idealized boundary conditions and/or short integration periods that make it difficult to evaluate deep ocean flows (e.g., Smith et al. 2000; Oschlies 2002; Treguier et al. 2005). This study aims to explore the gap between coarse and ocean eddy-resolving simulations in a series of centennial-time-scale global GCM simulations with horizontal resolutions ranging from coarse to ocean eddy-permitting. The focus is on the North Atlantic Ocean and in particular the North Atlantic climate response to the 8.2-kyr freshwater forcing event.

Corresponding author address: Paul Spence, Climate Change Research Centre, Level 4 Mathews Building, University of New South Wales, Sydney NSW 2052, Australia.
E-mail: paul.spence@unsw.edu.au

DOI: 10.1175/JCLI-D-11-00683.1

The 8.2-kyr event refers to widespread centennial-scale cooling found in paleoclimate records of the North Atlantic region roughly 8200 calendar years ago (Alley and Agustsdottir 2005; Rohling and Palike 2005). Paleoevidence suggests that the 8.2-kyr event coincides with the catastrophic drainage of roughly 1.65×10^{14} m^3 of freshwater from proglacial lakes Agassiz and Ojibway (hereafter referred to as Lake Agassiz) into Hudson Bay (Barber et al. 1999; Clarke et al. 2004). A wide range of coarse-resolution climate modeling studies demonstrate a reduction in meridional heat transport (MHT) by the Atlantic meridional overturning circulation (AMOC) in response to freshwater forcing at North Atlantic Deep Water (NADW) formation sites: more stably stratified surface water reduces NADW formation, which weakens the AMOC and its concomitant meridional heat transport, producing a cooling of North Atlantic climate (e.g., Stommel 1961; Stouffer et al. 2006). Consequently, this mechanism is commonly evoked to explain many large-scale climate events found in paleorecords, including the 8.2-kyr event (e.g., Bond et al. 1993; Rahmstorf 2002).

Coupled general circulation climate models have been employed at coarse resolutions in numerous studies to investigate the climate impact of a catastrophic drainage of Lake Agassiz into Hudson Bay. In particular, LeGrande et al. (2006) employ a coarse-resolution climate model that explicitly tracks water isotopes to find that a 40%–60% reduction in NADW produces isotopic signatures consistent with multiple paleoclimate proxies of the 8.2-kyr event. In contrast, Clarke et al. (2009) find that a massive Hudson Bay flooding event can rapidly cool the North Atlantic climate without a substantial reduction in poleward heat transport if one accounts for geographic differences in drainage sediment loading. Renssen et al. (2002) present evidence that the magnitude and duration of freshwater-induced climatic events may strongly depend on nonlinear dynamics within the coupled climate system. Also, Bauer et al. (2004) and Meissner and Clark (2006) find that the temporal evolution of the meltwater flux rates and the meltwater pathways during the final stage of the Laurentide Ice Sheet is important for simulating the magnitude and duration of North Atlantic cooling identified in paleoclimate records.

However, it has been widely noted that many oceanic processes that may be critical to the North Atlantic climate response to the Lake Agassiz discharge, such as boundary current flows and mesoscale eddies (e.g., Wunsch 2007; Lozier 2010), are poorly simulated by coarse-resolution climate models. Furthermore, these models typically simulate the flooding event by ''hosing'' large regions of the North Atlantic (e.g., between 50° and 70°N), disregarding the dynamical mechanisms responsible for transporting the freshwater from Hudson Bay to NADW formation regions (e.g., Renssen et al. 2002; Bauer et al. 2004; Stouffer et al. 2006). Unfortunately, only a limited number of studies have examined the effect of increasing model resolution on the North Atlantic climate and deep water formation response to freshwater perturbations.

Recently, Condron and Winsor (2011) highlighted the importance of resolving narrow coastal currents when assessing the impacts of coastal freshwater flooding. Simulating the 8.2-kyr flooding event with a 1/6° horizontal resolution ocean-ice model, Condron and Winsor (2011) found that freshwater released into Hudson Bay is initially confined to the continental shelf region of the Labrador Sea before being transported to the subtropical Atlantic, with little overall effect on North Atlantic open ocean salinity and convection. However, the study of Condron and Winsor (2011) is limited to an analysis of North Atlantic salinity within the 10-yr period after forcing, and does not address the AMOC or overall climate response to the freshwater discharge. Previously, Spence et al. (2008) found that the AMOC and surface air temperature (SAT) response of a global climate model to the 8.2-kyr event freshwater forcing had little sensitivity to an increase in horizontal resolution from 1.8° (latitude) × 3.6° (longitude) to 0.2° × 0.4°. However, there are two significant caveats to the results of Spence et al. (2008): 1) the ocean bathymetry was left unchanged as the model resolution was increased, and 2) a high value of ocean horizontal viscosity was employed. Both of these caveats are addressed here.

This study evaluates the decadal-scale climate impacts of a catastrophic drainage of Lake Agassiz with coarse and eddy-permitting versions of a global coupled climate model. Similar to Condron and Winsor (2011), the model simulations presented here are integrated under modern boundary conditions, and as such they are likely to be only marginally relevant to specifics of the 8.2-kyr event given that the simulations exclude of many forcings specific to the 8.2-kyr climate. For example, while the 8.2-kyr event conditions are not well known, the orbital forcing was different and sea level was likely 20 m lower than today, the global mean ocean salinity was likely higher, river runoff was likely quite different, and the atmospheric circulation would have been substantially influenced by the presence of large ice sheets (Licciardi et al. 1999). As such, theses simulations cannot readily be compared with proxy reconstructions, but they are useful to gauge the role of ocean model resolution in simulating the response to abrupt coastal meltwater events such as the 8.2-kyr event.

We begin with a brief overview of the climate model employed and the experimental design, followed by

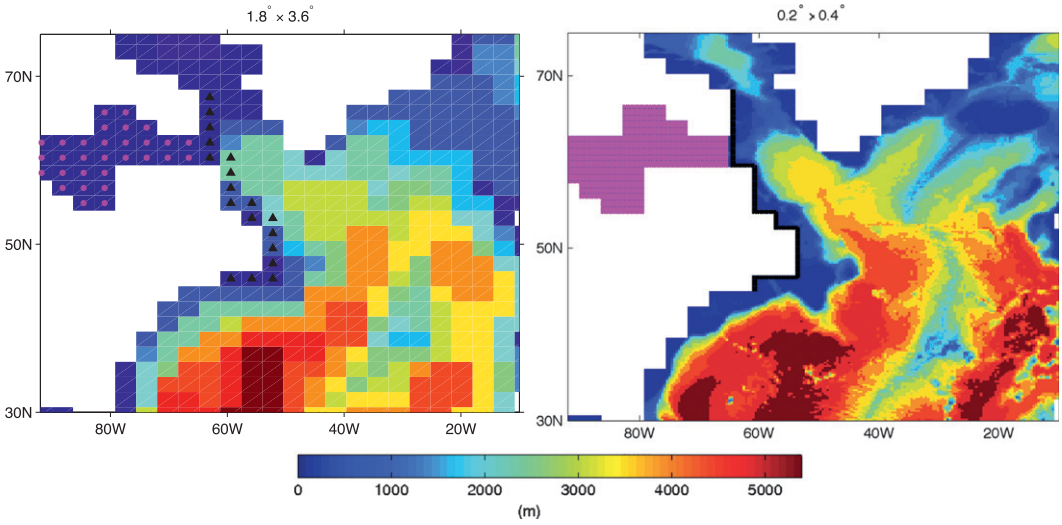

FIG. 1. (left) 1.8° × 3.6° and (right) 0.2° × 0.4° resolution bathymetry (m) in the North Atlantic employed by the simulations. Pink and black markers indicate regions of Hudson Bay (HBAY) and Labrador Current (LC) freshwater forcing, respectively.

discussions of the sensitivity of North Atlantic MHT, volume transport, and salinity advection to varying freshwater forcing scenarios and model resolutions. In general agreement with Condron and Winsor (2011), we find that discharging the freshwater within Hudson Bay initially mitigates the North Atlantic climate impact relative to an open ocean freshwater discharge scenario. However, the slow escape of freshwater from Hudson Bay leads to a stronger cooling response on longer time scales. We also find a greater maximum decline and a slower recover of the AMOC at higher resolution irrespective of the freshwater forcing region.

2. Model and experimental design

This study uses the University of Victoria Earth System Climate Model (UVic ESCM), which couples a simple vertically integrated energy–moisture balance atmospheric model, a thermodynamic/dynamic sea ice model, and a land surface model with the Geophysical Fluid Dynamics Laboratory (GFDL) Modular Ocean Model (MOM), version 2.2 (see Weaver et al. 2001 for details).

We employ two model versions, which have horizontal resolutions of 1.8° (latitude) × 3.6° (longitude) and 0.2° × 0.4°. Both versions have a global domain and all model components have the same horizontal grid resolution. The high-resolution model captures transient and stationary mesoscale features at scales larger than the baroclinic Rossby radius, which are prominent in the North Atlantic Ocean (Stammer 1997). The 0.2° × 0.4° model employs high-resolution bathymetry derived from the National Geophysical Data Center (NGDC) dataset (available online at http://www.ngdc.noaa.gov/mgg/fliers/93mgg01.html); however, the landmasses are held fixed to the 1.8° × 3.6° model grid (see Fig. 1). The coarse-resolution land/sea mask was used in the 0.2° × 0.4° simulation to avoid complications that can arise from flows through regions of complex coastal bathymetry (e.g., the Canadian archipelago); however, it also limits accurate representation of coastal currents in the high-resolution model. In both model versions the ocean model has 19 vertical levels and vertical diffusivity ranges from 3.0×10^{-5} m^2 s^{-1} near the surface to 1.3×10^{-4} m^2 s^{-1} at depth according to the scheme of Bryan and Lewis (1979).

The UVic ESCM employs a vertically integrated energy-moisture balance atmospheric model for computational efficiency. The winds are prescribed from the long-term monthly mean climatology of the National Centers for Environmental Prediction (NCEP)–National Center for Atmospheric Research (NCAR) 50-Year Reanalysis (Kistler et al. 2001) and interpolated to match model resolutions. While the wind fields are not dynamically resolved, atmospheric heat and moisture are fully coupled to the other model components. Atmospheric heat transport is parameterized by diffusion, and moisture is advected by the winds and diffused. Precipitation occurs when the relative humidity exceeds 90%, and land soil moisture is treated by a simple bucket model. The UVic ESCM is forced from startup by insolation and surface winds.

The high-resolution model was equilibrated for 100 years, starting from a long-term spinup of the 1.8° × 3.6°

version under preindustrial forcing conditions. This allows us to evaluate deep ocean flows in a near-equilibrium state of an ocean eddy-permitting, global climate model without idealized buoyancy fluxes. The integration of the ocean eddy-permitting models exceeds the thermocline adjustment time scale, but is not sufficient to remove all the long-time-scale transients in the deep ocean. To estimate the magnitude of model drift and interannual variability relative to the forcing response, the control-state simulations were concomitantly extended alongside the freshwater forcing simulations (see Figs. 3 and 6, described in more detail below). All of the anomalies presented here are determined by differencing the forced simulation from the extended control-state simulations. Thus, model drift is accounted for in a linear sense by differencing forced and control runs that have undergone the same integration time. Given the large magnitude of freshwater forcing from Lake Agassiz, the amplitude of the North Atlantic climate response over roughly the first three decades is larger than the control-state model drift and interannual variability in both models.

Model parameter specifics and the North Atlantic control-state climate of these simulations are described in detail in Spence et al. (2012), where the corresponding $0.2° \times 0.4°$ model is labeled as the low A_M or the ''lower viscosity'' simulation. Here, we briefly note that the 1.8 PW of total oceanic MHT at 24°N in the high-resolution simulation is within the observational estimate of Ganachaud and Wunsch (2003), and presents a 33% increase relative to the coarse-resolution simulation. The increased heat transport is attributed to the improved resolution large-scale ocean currents at higher resolution (Fig. 2; see also Smith et al. 2000; Treguier et al. 2005). At 50°N the zonal width of one grid box at $1.8° \times 3.6°$ is 255 km, while at $0.2° \times 0.4°$ it is 28 km wide. The high-resolution model is therefore able to resolve the width of the Labrador shelf (95–175 km) and also the branches of Labrador Current, which are observed to be roughly 100 km wide (Flatau et al. 2003; Lazier and Wright 1993). The first baroclinic Rossby radius of deformation is about 17 km at 50°N (Chelton et al. 1998).

The maximum near-surface current speed of the Gulf Stream at 68°W increases from 13 cm s^{-1} at $1.8° \times 3.6°$ to 67 cm s^{-1} at $0.2° \times 0.4°$ (Fig. 2, top), with observed estimates in this region of 70 cm s^{-1} (Johns et al. 1995). The maximum near-surface speed of the Labrador Current near 55°W increases from 4 to 16 cm s^{-1} between the $1.8° \times 3.6°$ and the $0.2° \times 0.4°$ simulations, with observed values of roughly 30 cm s^{-1} (Flatau et al. 2003). Note that, similar to the observations of Lazier and Wright (1993), the colored velocity field of Fig. 2 reveals that the Labrador Current in our high-resolution simulation has a near-shore continental shelf branch and an offshore continental slope branch, both of which are roughly 100 km wide. Figure 2 (bottom) shows the control-state North Atlantic barotropic streamfunction in both models. In the control state, we note the following attributes of the $0.2° \times 0.4°$ simulation relative to the coarse simulation: 1) western boundary transports are intensified and better constrained to the continental shelf region; 2) small-scale recirculations are evident, particularly along the northern edge of the subtropical gyre; 3) there is improved poleward penetration of the North Atlantic Current (NAC); and 4) the subpolar gyre penetrates farther into the Labrador Sea, increasing transport in the region. These attributes are consistent with results from other resolution sensitivity studies (e.g., Willebrand et al. 2001; Treguier et al. 2005). While many features of the North Atlantic horizontal circulation are shown to be improved at higher resolution, some important features remain poorly simulated. In particular, we note that the Gulf Stream separates from the coastline too far north and the near-shore branch of the Labrador Current is forced to follow a poorly resolved coastline in the $0.2° \times 0.4°$ simulation.

Two forcing regions are considered at both model resolutions (see Fig. 1). In the first scenario (hereafter referred to as LC forcing), we follow Spence et al. (2008) and apply the freshwater forcing within the Labrador Current region along the coastline of northeast North America. At $1.8° \times 3.6°$ the zonal width of the LC forcing is one grid box wide (255 km wide at 50°N), whereas at $0.2° \times 0.4°$ it is two grid boxes wide (56 km wide at 50°N). Condron and Winsor (2011) estimate that the freshwater pulse had a width of 40–100 km along the Labrador Shelf, which is within the high-resolution LC forcing range. In the second scenario (hereafter referred to as HBAY forcing), the freshwater is applied directly within Hudson Bay.

The use of a rigid-lid approximation in the ocean model requires surface freshwater fluxes to be converted to a virtual ocean surface salt flux with a constant salt-to-freshwater mass ratio that excludes any direct influence of the freshwater forcing on ocean temperature. Virtual salt fluxes can lead locally to negative salinity values where a strong external freshwater forcing (or salt removal) is applied over a relatively small volume. To prevent this, the freshwater perturbation associated with the catastrophic drainage of Lake Agassiz is simulated as a 3-yr, 1.75-Sv ($1 \text{ Sv} \equiv 10^6 \text{ m}^3 \text{ s}^{-1}$) surface freshwater flux anomaly. Note that paleoevidence suggests that the catastrophic drainage of Lake Agassiz occurred in a year or less (Clarke et al. 2004). The same total virtual salt flux anomaly is applied in each forcing simulation, irrespective of differences in the forcing region.

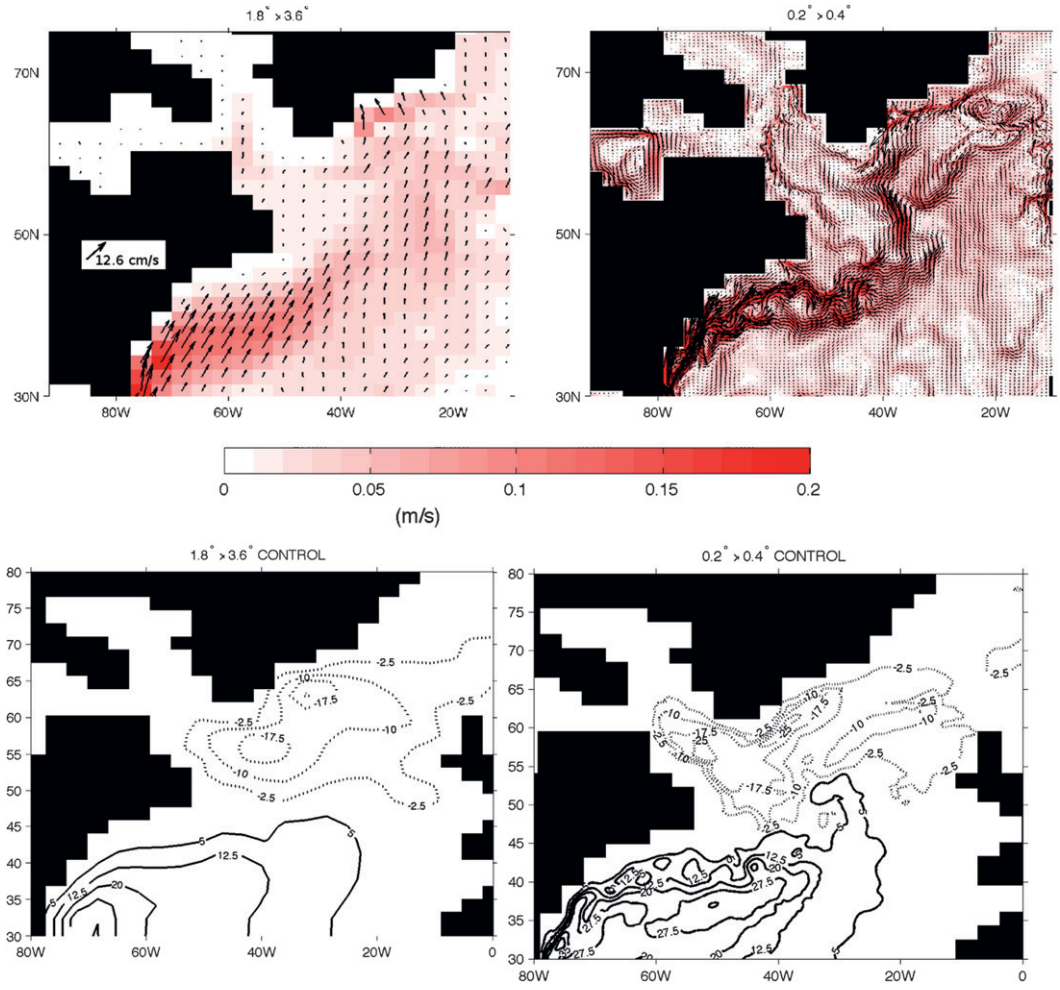

FIG. 2. (top) Control-state annual mean North Atlantic velocity field at 126-m depth in the (left) 1.8° × 3.6° and (right) 0.2° × 0.4° simulation. Only vectors at every second grid point are plotted for the 0.2° × 0.4° simulations to aid clarity. The velocity fields are normalized to the scaling vector shown at left. Colors show 5-yr mean absolute velocity field. (bottom) Contour lines (solid clockwise and dashed counterclockwise flow) of 5-yr mean barotropic streamfunction in model control states in the (left) 1.8° × 3.6° and (right) 0.2° × 0.4° simulation (contour interval: 7.5 Sv).

Inaccuracies can arise from virtual salt fluxes in regions where the local sea surface salinity (SSS) is substantially different from the reference salinity (e.g., in Siberian river mouths where the SSS is often less than 20 g kg^{-1}). However, virtual salt fluxes do a reasonable job of parameterizing the effects of freshwater on tracer concentration in regions where the globally constant reference tracer concentration is close to the local concentration (Griffies et al. 2005). In our simulations the reference salinity is 34.9 g kg^{-1}, and the mean SSS salinity in Hudson Bay is 33.0 and 34.3 g kg^{-1} in the 1.8° × 3.6° and the 0.2° × 0.4° control simulations, respectively. Since the SSS in the forcing region of the models is close to the reference salinity, inaccuracies related to the use of virtual salt flux are unlikely to be a primary cause of the large differences we find between the simulations.

In these experiments the freshwater released from Lake Agassiz is assumed to be in liquid form, and consequently it should be released close to the Lake Agassiz source region. On the other hand, if the freshwater forcing is assumed to be mostly in the form of ice, then one could conceivably ''spread it out'' over the whole subpolar Atlantic, as in Stouffer et al. (2006). However, for the latter scenario to be consistent with its own assumptions, one should come up with an adequate hypothesis as to where the heat required to melt the ice comes from. For example, to melt 1 Sv of ice requires a supply of about 0.3 PW of heat. This is a huge amount of heat loss and it could significantly modify the ocean/climate response. We note that this heat loss is often ignored in the hosing experiments that adopt the ''uniform'' approach for distribution of freshwater forcing.

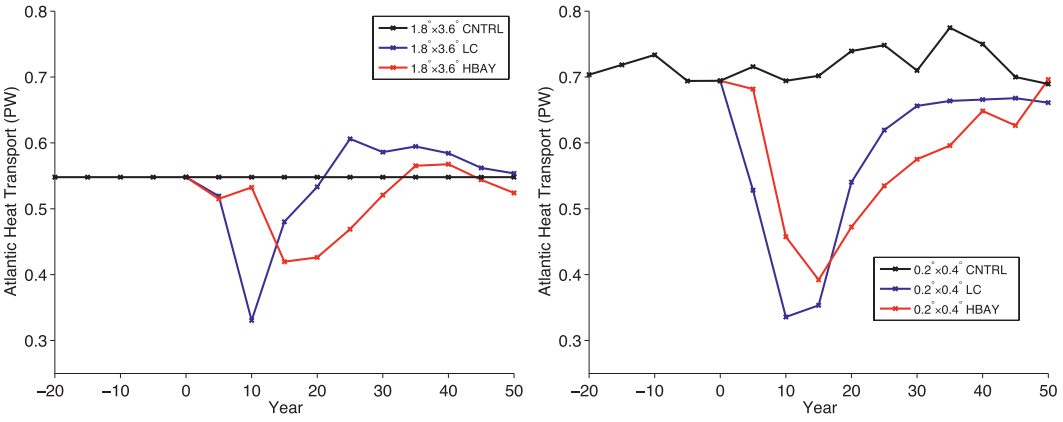

FIG. 3. North Atlantic time-mean meridional heat transport at 45°N in the (left) 1.8° × 3.6° and (right) 0.2° × 0.4° control-state simulation and in response to the freshwater forcing scenarios.

3. Results

a. Meridional heat transport

Observational estimates suggest that outside of low latitudes most of the MHT in the climate system is carried within the atmosphere (Trenberth and Caron 2001). In spite of its relative size, changes in oceanic heat transport can have a profound influence on climate (Saenko 2009). Figure 3 shows time series of 5-yr mean Atlantic MHT at 45°N in the control state of the simulations and in response to the freshwater forcing scenarios. The long-term average control-state Atlantic MHT at 45°N increases from 0.55 PW with negligible variability at 1.8° × 3.6° to 0.72 PW with a standard deviation of ±0.03 PW at 0.2° × 0.4°. As previously discussed, the increase in MHT at 0.2° × 0.4° can be attributed to the enhanced resolution of the large-scale ocean currents. The MHT response to the freshwater forcing is consistent in that all four simulations exhibit an initial reduction in MHT that far exceeds the control-state MHT variability, followed by a recovery trajectory. However, the amplitude and trajectory of the MHT anomalies to the freshwater are sensitive to model resolution and forcing region. In particular, at a given model resolution the MHT initially has a smaller response to HBAY forcing than to LC forcing, but on longer time scales (>15 yr) the HBAY forcing anomaly is consistently larger. Five years after forcing the MHT anomaly is consistently larger at high resolution than coarse resolution for a given forcing scenario, with percent differences between the coarse- and high-resolution anomalies at 5-yr intervals in the range of 45%–55%.

The simulated surface air temperature response area weighted between 40° and 80°N and 100°W and 30°E in the North Atlantic (Fig. 4 top, right) is consistent with the MHT response. At coarse resolution, the LC response is characterized by an initial (<15 yr) cold phase followed by a longer-term (>30 yr) period of slightly warmer North Atlantic climate, while the HBAY simulation is characterized by a relatively weak cooling response. In contrast, both high-resolution simulations remain in a cold phase throughout the transient runs, with HBAY cooling being larger than LC cooling after roughly 18 years. The 50-yr mean SAT anomaly at coarse resolution is −0.16°C and −0.05°C for HBAY and LC forcing, respectively, while at high resolution the 50-yr mean anomaly is −0.45°C for both forcings.

Changes in sea ice volume corroborate the trends identified in the SST and MHT response (Fig. 4 bottom, left). In particular, over the 50-yr transient period the high-resolution model has a roughly 18% increase in North Atlantic sea ice volume for both forcings, while the coarse-resolution model actually loses an average of 4% and 13% in the HBAY and LC simulations, respectively. SST anomalies under the North Atlantic sea ice increases further corroborate the sea ice response (Fig. 4 bottom, right). The substantial reduction in North Atlantic sea ice for 1.8° × 3.6° LC forcing simulation is intriguing. Figure 4 (bottom, right) shows that the SST anomalies located under North Atlantic sea ice corroborate the sea ice volume response of each simulation. A closer analysis of the 1.8° × 3.6° LC simulation reveals that a localized warming signal occurs in the sea ice region of the southern Greenland Sea by year 15. The mechanism for this warming is similar to that identified by Saenko et al. (2007) in that the LC forcing in this case brings warmer and saltier ocean waters from depth to the upper surface by tilting isopycnal slopes. We are uncertain why this mechanism is prominent in this particular simulation and not others.

A large-scale cooling of North Atlantic climate in response to freshwater forcing in models is most often

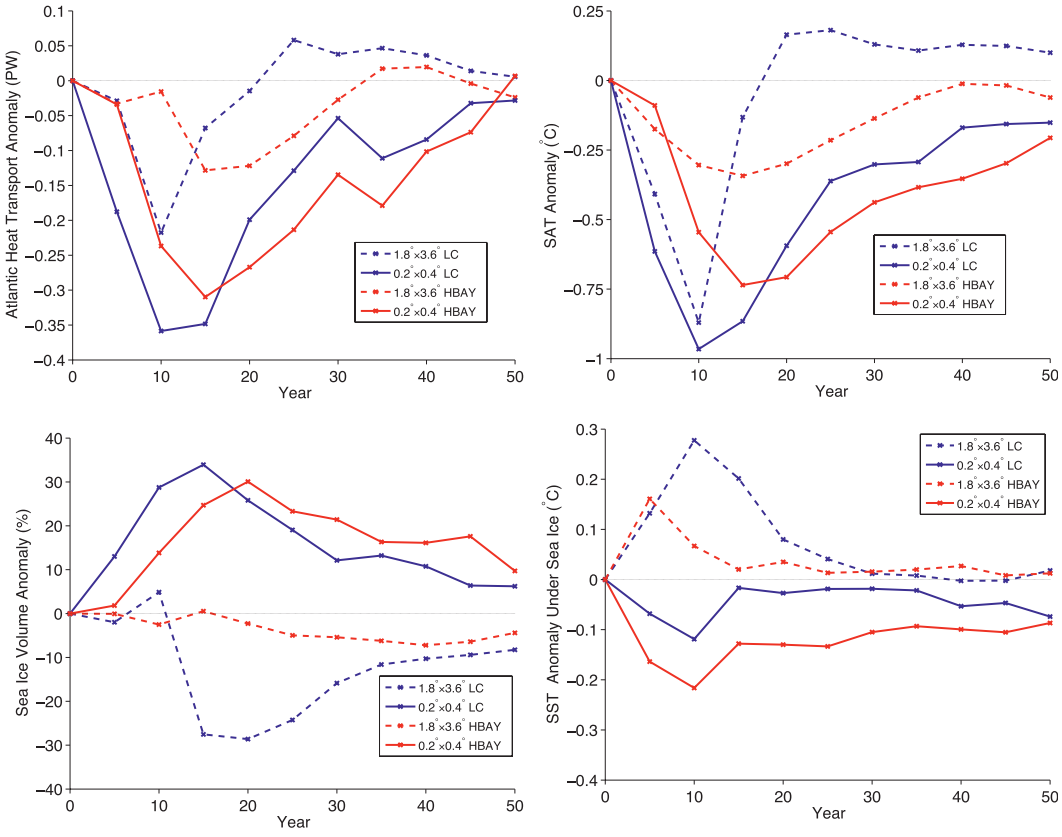

FIG. 4. (top, left) North Atlantic meridional heat transport anomaly (PW) at 45°N. (top, right) Surface air temperature (SAT; °C) and (bottom, left) sea ice volume anomaly (%), both of which are area weighted between 40° to 80°N and 100°W to 30°E in the Atlantic. (bottom, right) SST anomalies under North Atlantic sea ice. All values are determined from 5-yr time averages.

attributed to a weakening of MHT by the time-mean overturning circulation (e.g., Teller et al. 2002; Condron and Winsor 2011). However, numerous studies attribute improvements in the simulation of North Atlantic MHT at higher resolution to an increase in transport by the time-mean gyre circulation (e.g., Fanning and Weaver 1997; Bryan and Smith 1998; Spence et al. 2008). In turn, freshwater forcing induced changes in the MHT by the time-mean gyre circulation may be significant at high resolution. Furthermore, while the large-scale ocean heat transport appears to be dominated by the mean circulation (Wunsch 1999; Talley 2003), heat transport by small-scale and time-varying circulations can locally be of first-order importance, and may influence the large-scale heat transport indirectly by modifying the mean flow and surface heat flux budgets (Stammer 1997). In the interest of determining what sets the MHT response we decompose the North Atlantic MHT into components associated with the time-mean and transient processes of the gyre and overturning circulations.

Following Bryan (1982), and adopting the notation of Volkov et al. (2010), the net MHT $\overline{Q}(y)$ can be decomposed as follows:

$$\overline{Q}(y) = \iint \rho C_p \{[\overline{v}][\overline{\theta}] + \overline{[v'][\theta']} + (\overline{v})(\overline{\theta}) + \overline{(v')(\theta')}\}\, dz\, dx, \tag{1}$$

where ρ is the potential density of sea water, C_p is the specific heat content at constant pressure, and $v(x, y, z, t)$ and $\theta(x, y, z, t)$ are the meridional velocity and potential temperature, respectively. The overbar indicates averaging in time, whereas the prime represents the deviation from the corresponding time-mean field; $[\cdot]$ denotes zonal averaging, whereas $(\cdot)$ represents the deviation from the zonal average. The four terms on the right-hand side of Eq. (1) are caused by 1) the time-mean overturning circulation, 2) the transient processes in the overturning circulation, 3) the time-mean horizontal (or "gyre") circulation, and 4) the transient processes in the horizontal (gyre) circulation. In these calculations, v and

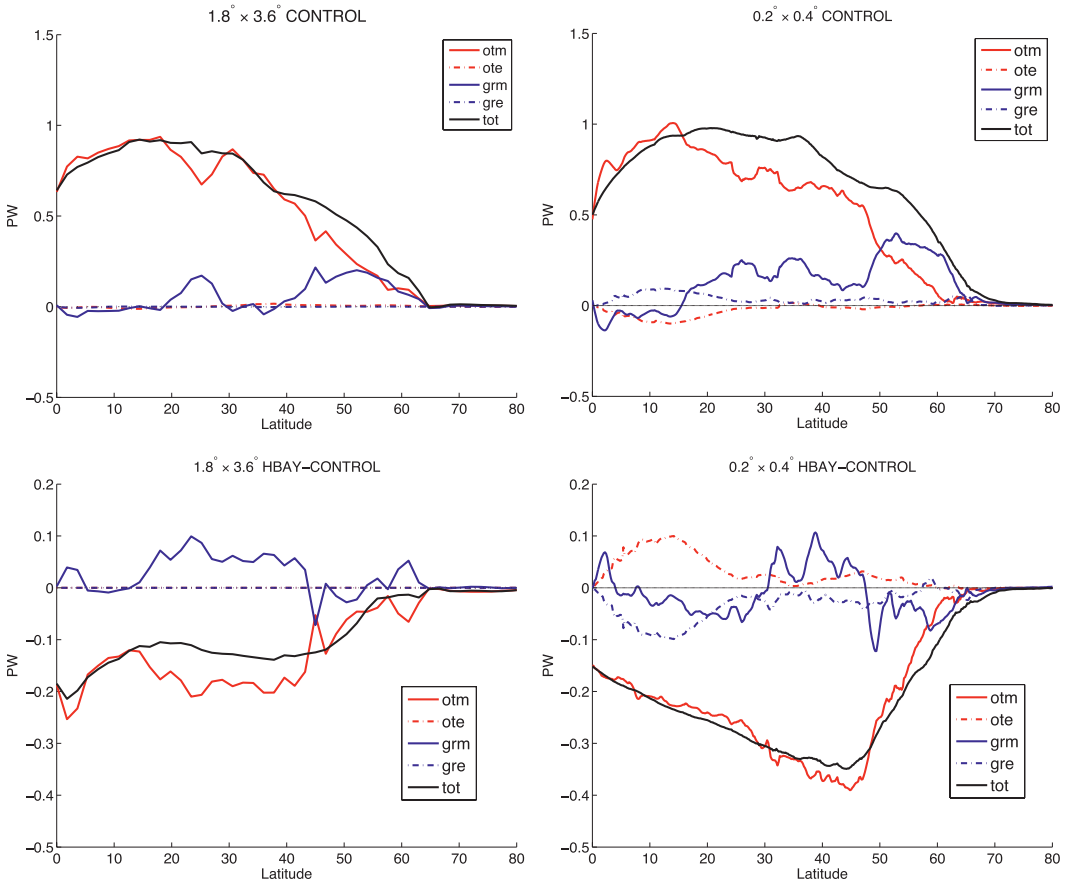

FIG. 5. (top) Zonal averaged Atlantic meridional heat transport components in control states in the (left) 1.8° × 3.6° and (right) 0.2° × 0.4° simulation and (bottom) anomalies 20 years after HBAY forcing is initiated in the (left) 1.8° × 3.6° and (right) 0.2° × 0.4° simulation. The total MHT (tot) and its components caused by the time-mean meridional overturning (otm), the overturning transients (ote), the time-mean horizontal circulation (grm), and the horizontal transients (gre) are shown. All values are determined from snapshots taken at 5-day intervals over 1 yr.

θ are represented by their instantaneous snapshots recorded at 5-day intervals over a 1-yr period. We evaluate the MHT components in the control state of both models and anomalies in response to the HBAY forcing scenario, which are generally consistent with LC forcing results.

Figure 5 (top) shows the contributions of each component to the net North Atlantic MHT in the control state of the models. In agreement with previous studies (e.g., Smith et al. 2000; Treguier et al. 2005), it reveals an increase in the net MHT poleward of roughly 35°N at higher resolution relative to coarser resolution. In both models, the overturning mean component is the dominant transport mechanism between 0° and 45°N, while the gyre mean component plays a large role poleward of 45°N. The increased MHT at higher resolution can largely be attributed to an increase in the gyre mean transport, which results from improvements in the simulation of the large-scale currents (refer to section 2). There is also a slight increase in the overturning mean component between 35° and 45°N and a slight decrease between roughly 25° and 35°N at higher resolution that can be attributed to a poleward shift of the maximum AMOC transport (see Fig. 7). The contribution of transients to the net MHT is relatively small.

Figure 5 (bottom) shows the HBAY forcing–induced MHT anomalies at year 20. At coarse resolution, the decline in net MHT is predominately dictated by changes in the overturning mean component. The same is true in the high-resolution simulation except poleward of roughly 45°N, where the gyre mean component provides a substantial contribution to the net decline. Significant transient overturning and gyre component anomalies are found equatorward of 25°N at high resolution, but they tend to compensate each other with little overall impact on the net MHT change.

b. *Volume transport*

The zonally integrated control-state AMOC of the coarse- and high-resolution models reveals similar rates

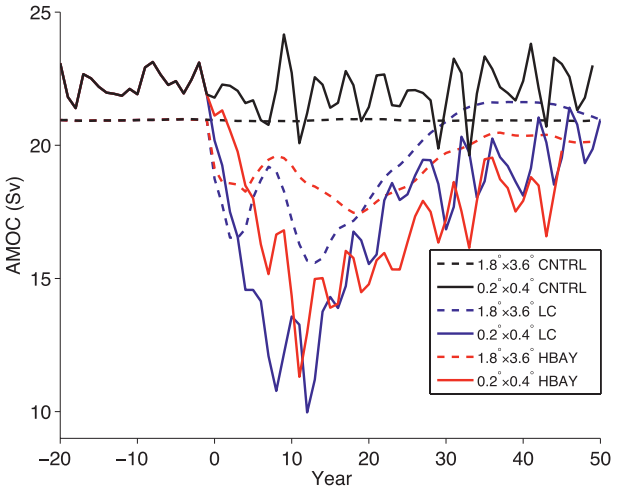

FIG. 6. Maximum annual mean AMOC transport (Sv) in the model control states and in response to 3 yr of 1.75-Sv freshwater forcing beginning at year 0. Calculated as the maximum meridional overturning streamfunction transport between 26° and 70°N and 170–4000-m depth in the Atlantic.

of NADW production and a common structure (Figs. 6 and 7). The control-state AMOC transport in the 1.8° × 3.6° simulation is 21 Sv with little internal variability, while the 0.2° × 0.4° simulation has a mean transport of roughly 22 Sv with interannual variability of roughly ±2 Sv. The relatively low interannual variability in the AMOC transport of the UVic ESCM simulations may be partially attributed to the simple atmospheric component with fixed monthly mean wind fields. Observational estimates of present-day AMOC transport range from 13 to 23 Sv (e.g., Ganachaud and Wunsch 2000; Smethie et al. 2000). It is worth noting the different transport pathways of recently ventilated NADW into the subtropics between the simulations. NADW in the coarse-resolution model predominantly follows the deep western boundary current (DWBC) to the subtropics, whereas in the high-resolution model much of the NADW separates from the western boundary near the Grand Banks and enters the low-latitude Atlantic via interior pathways distinct from the DWBC (see Fig. 7 of Spence et al. 2012). The importance of interior NADW pathways into the subtropics has been highlighted in recent observational studies (Lozier 2010), and bottom pressure torques are found to play an important role in these interior NADW outflows (Spence et al. 2012).

In response to the freshwater forcing scenarios, both the coarse- and high-resolution models exhibit a reduction in AMOC transport followed by a recovery trajectory (Figs. 6 and 7). Similar AMOC response sensitivities to those identified for MHT are clearly evident: 1) for a given model resolution, the AMOC initially (i.e., ≤10 yr) exhibits a weaker response to HBAY forcing than to LC forcing; 2) on longer time scales (i.e., ≥20 yr) the HBAY forcing anomaly is consistently larger than the LC forcing anomaly for a given model resolution; and 3) for both forcing scenarios the maximum reduction in AMOC transport is substantially larger at high resolution than at coarse resolution. In particular, averaged over the first 20 years of the HBAY simulation the AMOC at 1.8° × 3.6° is reduced by 10% (or 17% for LC forcing), while at 0.2° × 0.4° it is reduced by 24% (or 32% for LC forcing). The maximum AMOC transport decline for HBAY (LC) forcing increases from 17% (25%) at coarse resolution to 40% (53%) at high resolution. While the maximum AMOC transport declines under the freshwater forcing in all simulations, the AMOC largely maintains its latitudinal position and depth profile (Fig. 7).

Using a linear vorticity balance, $\beta v = f(\partial w/\partial z)$ (where f is the Coriolis parameter, $\beta \equiv \partial f/\partial y$, and w is the vertical velocity), changes in the meridional deep water flows (that integrate to form the lower branch of the AMOC) can be related to the corresponding components in the gyre circulation. Given that both models have the same time-invariant wind stress curl, they also have the same Sverdrup transport, typically confined to the upper ocean by stratification. At high resolution, however, the zonal structure of the AMOC lower branch is largely maintained by the bottom pressure torques (Spence et al. 2012). Since these torques could change in response to the freshwater forcing and to the associated density changes, it is of interest to examine the corresponding impact on both the gyre and the overturning circulations.

Figure 8 shows the North Atlantic barotropic streamfunction anomaly induced by HBAY forcing in both models. The large horizontal viscosity required at coarse resolution confines the barotropic circulation to a Sverdrup balance, wherein the wind stress is the primary forcing agent and bottom pressure torque is unimportant. In a Sverdrup balance state, changes in the ocean density structure by freshwater forcing can be expected to have little impact on the barotropic transport. Since the wind stress is held constant, the freshwater forcing induced barotropic anomaly is indeed shown to be weak in the coarse-resolution model. In contrast, a substantial barotropic anomaly pattern is evident in the high-resolution simulation, despite the unchanged wind stress curl. In particular, the barotropic transport within the western portion of the subpolar gyre and also within the Gulf Stream region decreases by more than 10 Sv, and a large anticyclonic recirculation that exceeds 20 Sv is found in the central North Atlantic. Bottom pressure torque plays

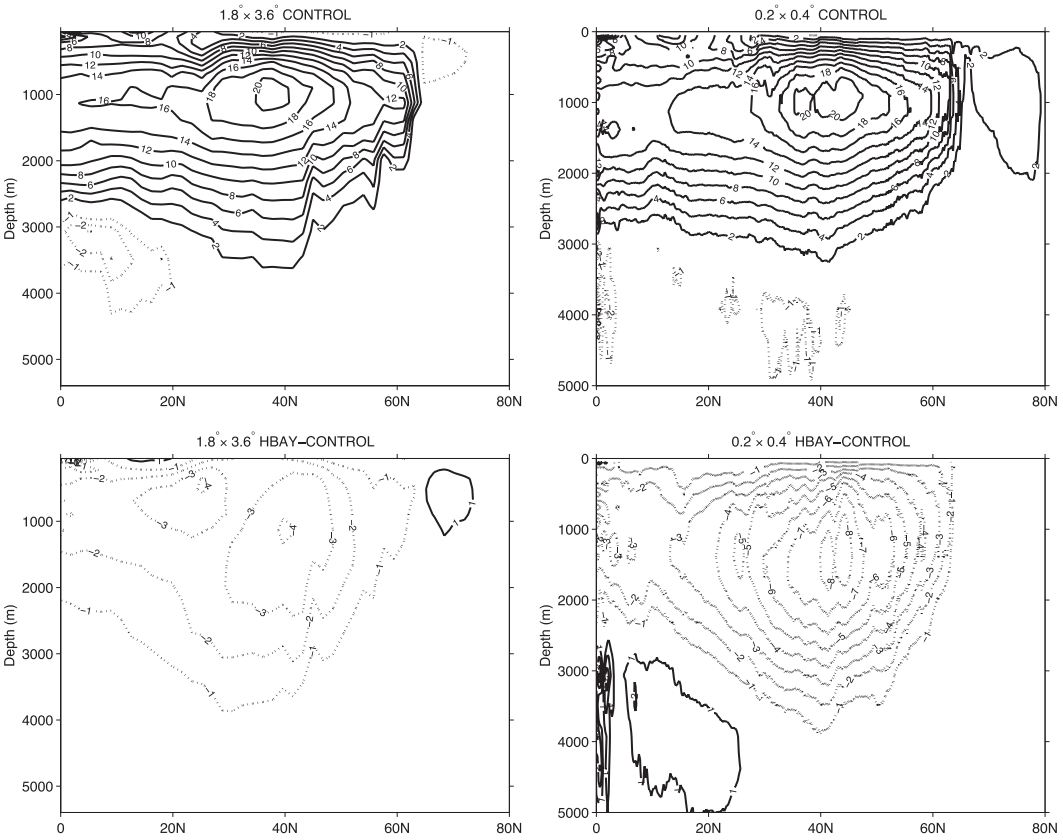

FIG. 7. (top) Five-year mean AMOC in model control states (contour interval: 2 Sv) in the (left) 1.8° × 3.6° and (right) 0.2° × 0.4° simulation and (bottom) average anomalies (contour interval: 1 Sv) for years 16–20 after HBAY forcing begins in the (left) 1.8° × 3.6° and (right) 0.2° × 0.4° simulation.

a key role in the linear vorticity balance of the 0.2° × 0.4° simulation (Spence et al. 2012), and the large barotropic anomaly provides evidence of the importance of bottom pressure torque in the freshwater forcing response.

c. *Salinity advection*

Many of the differences in the North Atlantic climate response to Lake Agassiz discharge found in the four

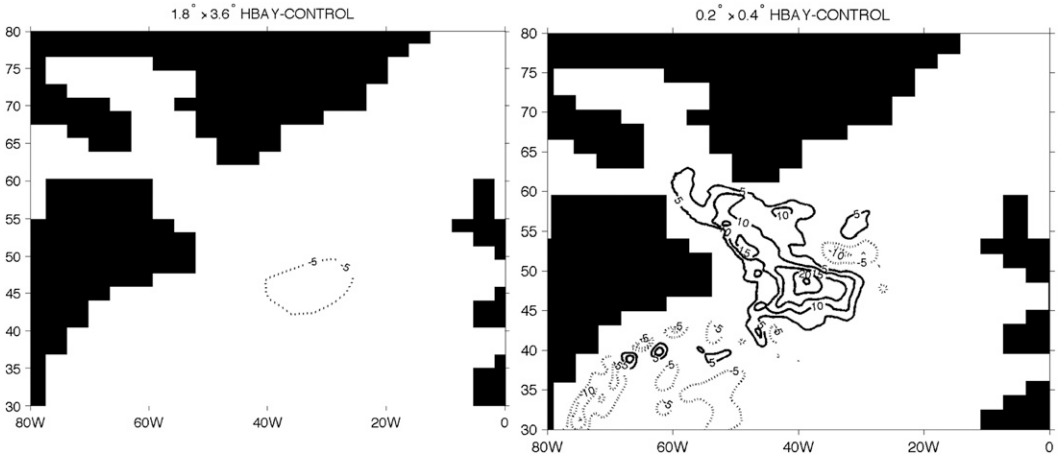

FIG. 8. Contour lines (solid clockwise and dashed counterclockwise flow) of 5-yr mean barotropic streamfunction anomalies (5-Sv contours) 16–20 years after initial HBAY forcing in the (left) 1.8° × 3.6° and (right) 0.2° × 0.4° simulation. Note that Fig. 2 (bottom) shows the control-state barotropic streamfunctions.

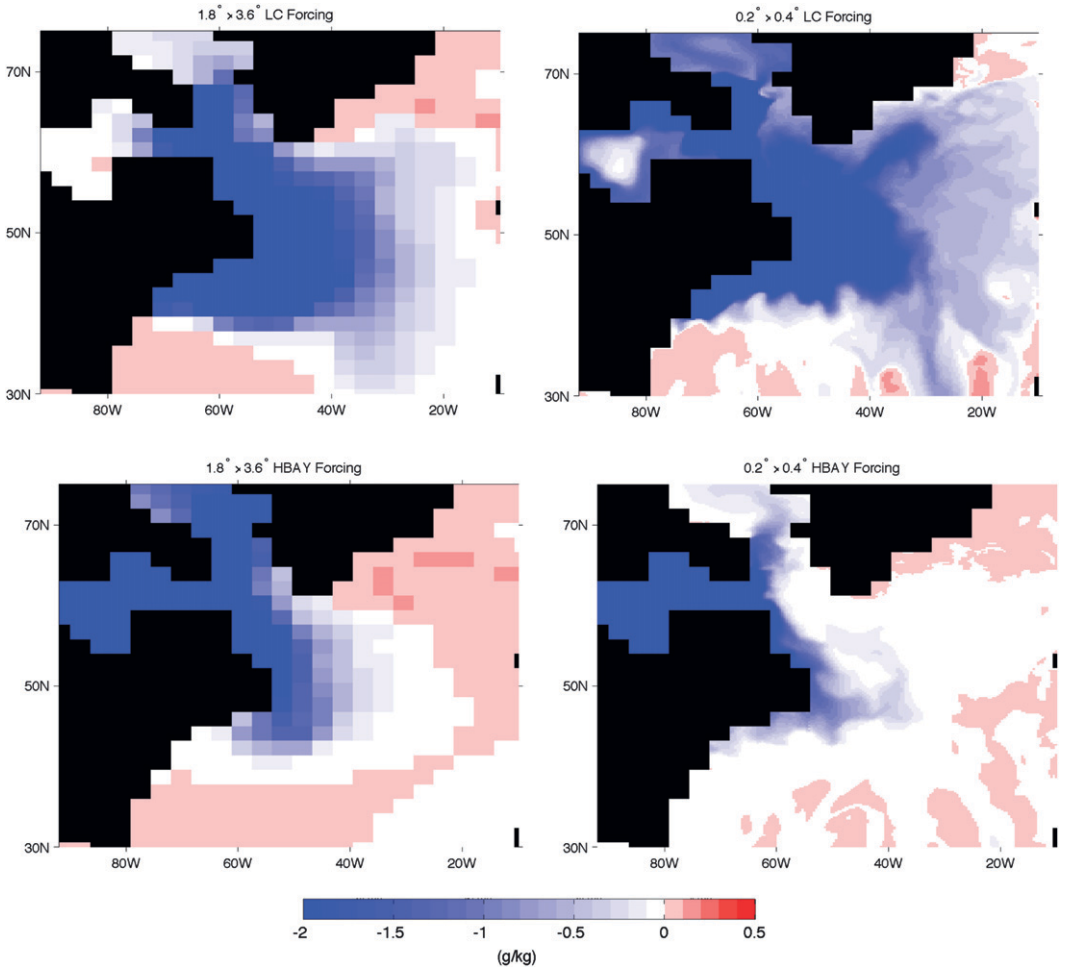

FIG. 9. Average North Atlantic salinity anomaly (g kg^{-1}) over years 1–5 of each freshwater forcing simulation within the top vertical ocean level for the (top) LC forcing in the (left) 1.8° × 3.6° and (right) 0.2° × 0.4° simulation and (bottom) HBAY forcing in the (left) 1.8° × 3.6° and (right) 0.2° × 0.4° simulation.

simulations can be attributed to differences in the advection of SSS anomalies. SSS anomalies averaged over the first and last 5 years of the 50-yr forcing runs reveal that, as one may expect, freshwater released into Hudson Bay persists far longer in the North Atlantic than freshwater released into the open ocean (Figs. 9 and 10). In turn, the greater long-term cooling found in the HBAY scenario relative to the LC scenario may be attributed to the slow escape of freshwater from Hudson Bay. It is also clear, particularly for HBAY forcing, that the freshwater discharge is more constrained to the continental shelf of the western Labrador Sea at higher resolution. The influence of freshwater confinement to the western boundary is further evidenced in Fig. 11, showing the temporal evolution of the North Atlantic zonal average SSS anomaly as a function of latitude.

As previously discussed, in their 10-yr 1/6° resolution simulation Condron and Winsor (2011) find that a subtropical fate awaits a Lake Agassiz discharge by flowing inshore of the Gulf Stream or following the Canary Current, with little overall effect on subpolar North Atlantic salinity and convection. Similar equatorward freshwater pathways are evident in the high-resolution SSS anomalies presented here, with low SSS anomalies found both inside the Gulf Stream and along the Canary Current (Figs. 9 and 10). However, a substantial portion of the freshwater anomaly is found to follow the North Atlantic Current poleward. Figure 11 demonstrates that the low SSS anomaly has spread equatorward to 20°N and poleward of 70°N by year 10 in the simulations. However, on longer time scales low SSS anomalies tend to persist in the subpolar region at high resolution, and in the subtropics at coarse resolution.

Note again the peculiar case of the 1.8° × 3.6° LC simulation, where after 15 years the SSS of the subpolar North Atlantic has increased (Figs. 10 and 11). In the

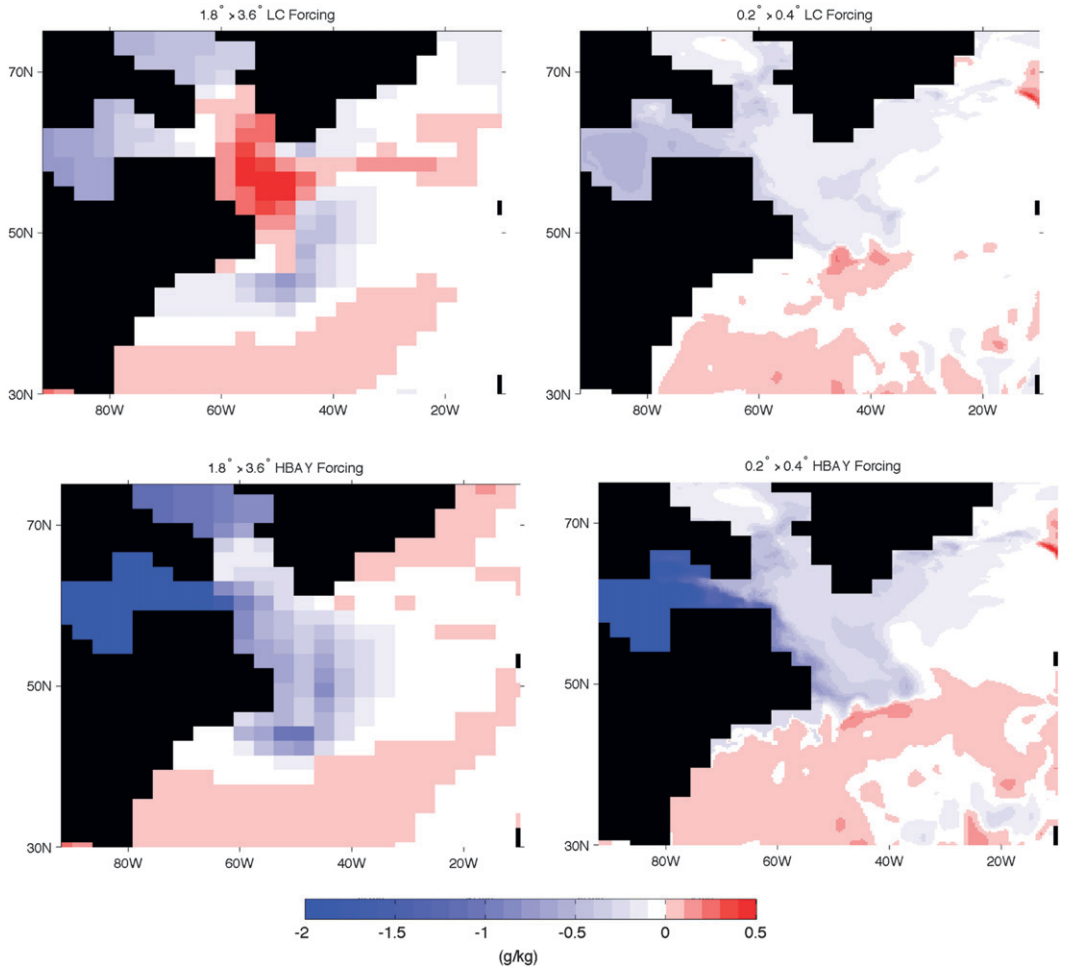

FIG. 10. Average North Atlantic salinity anomaly (g kg^{-1}) over years 46–50 of each freshwater forcing simulation within the top vertical ocean level for the (top) LC forcing in the (left) 1.8° × 3.6° and (right) 0.2° × 0.4° simulation and (bottom) HBAY forcing in the (left) 1.8° × 3.6° and (right) 0.2° × 0.4° simulation.

1.8° × 3.6° LC simulation, the freshwater anomaly is quickly advected to the eastern subpolar North Atlantic and then follows the NAC and Canary Current to the Arctic and subtropics. In contrast, in the 0.2° × 0.4° LC simulation the freshwater anomaly persists for several decades in the subpolar North Atlantic because of entrainment along the continental boundary and within Hudson Bay. Note that the peculiar SSS increase found in the 1.8° × 3.6° LC simulation initially begins as a localized anomaly in the southern Greenland Sea, much like the SST anomaly previously discussed (see Fig. 4 bottom, right). Again, in this simulation the boundary current forcing acts to tilt the isopycnals in the southern Greenland Sea region, which brings warm and salty ocean waters from depth to the surface (Saenko et al. 2007). In the fully coupled model of Saenko et al. (2007) this was also a result of changes in the wind stress curl and the associated changes in the Ekman pumping.

It is of interest to evaluate the role of transient processes in transporting freshwater from the discharge source region. This can be done by decomposing the vector of the net freshwater transport into its time-mean $(\overline{uq}, \overline{vq})$ and transient $(\overline{u'q'}, \overline{v'q'})$ components, where u is the zonal velocity and $q = 1 - S/S_R$ and $S_R = 34.9$ g kg^{-1} are the freshwater content and reference salinity, respectively. In these calculations, v, u, and S are represented by instantaneous snapshots recorded at 5-day intervals over a 1-yr period, excluding v induced by the Gent and McWilliams (1990) isopycnal thickness diffusion tracer mixing coefficient. We evaluate the MHT components in the control state of both models and in response to HBAY forcing, which is generally consistent with the LC forcing results.

Figure 12 shows vectors of the mean and transient freshwater transport at year 10 of the high-resolution HBAY simulation along with their zonal transport

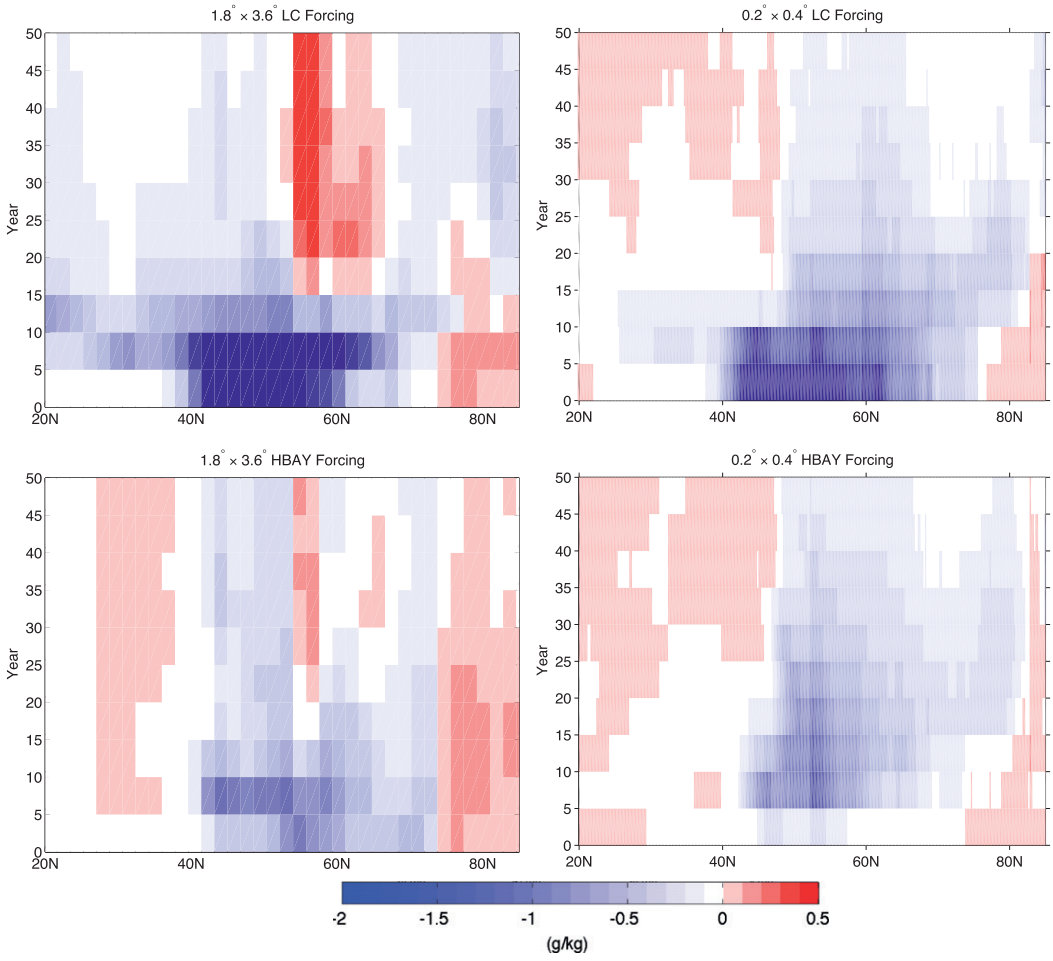

FIG. 11. Hovmöller plot of the temporal evolution of zonal average North Atlantic surface salinity anomalies within the top vertical ocean level as a function of latitude. Determined from 5-yr average salinity data. The zonal average is taken from 100°W to 30°E, which excludes Hudson Bay. (top) LC in the (left) 1.8° × 3.6° and (right) 0.2° × 0.4° simulation, and (bottom) HBAY in the (left) 1.8° × 3.6° and (right) 0.2° × 0.4° simulation.

components. The freshwater transport by the mean flow is shown to be at least an order of magnitude greater than the transient freshwater transport, which is similar to the ratio between mean and transient components of North Atlantic heat transport. While the transient freshwater transport contribution is generally weaker than the mean, transients do transport a large amount of freshwater from the coast into the interior between 50° and 60°N, and this effect may be expected to increase in eddy-resolving simulations. The main pathway for the freshwater to escape the boundary is between 45° and 50°N, where the mean transport is the largest.

The transport of low-salinity water throughout the North Atlantic can influence NADW formation by creating more stably stratified surface water, which reduces deep convective mixing. The methods used to parameterize convective mixing processes in models are widely debated (e.g., Treguier et al. 2005). The UVic ESCM employs an explicit full convection scheme, which includes diagnostics to save the ventilation depth and potential energy released by convection at each grid point (Pacanowski 1996). Here, we analyze changes in the freshwater content of surface waters at North Atlantic deep convection sites. In the control state of both models deep convective activity occurs predominately in the Greenland–Iceland–Norwegian (GIN) Seas, albeit too far south, and without a significant amount of interannual variability. In the coarse model, 95% of the control-state winter season (January–March) deep convection (i.e., with ventilation depths > 300 m) convective potential energy is released in the GIN region, with the remainder occurring in the Labrador Sea. At high resolution the fraction of Labrador Sea convection is increased to roughly 10%. Given the lack of Labrador

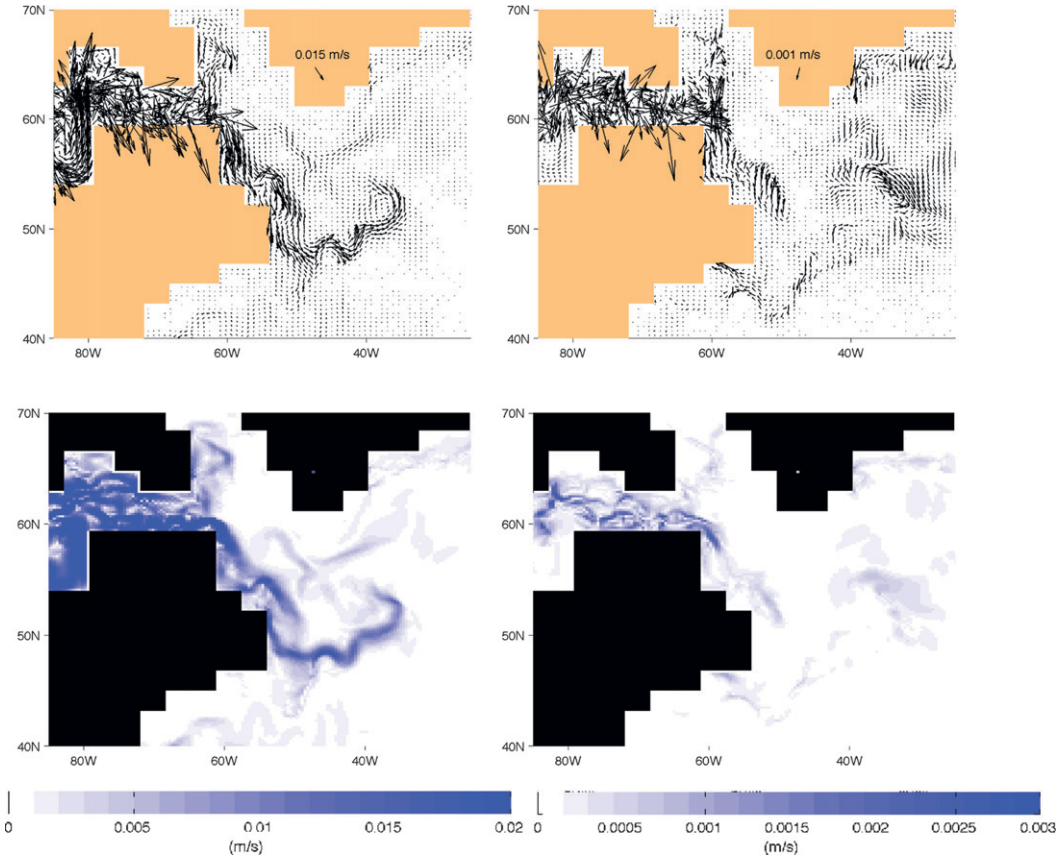

FIG. 12. (top) Vector field of surface freshwater transport by (left) mean and (right) transient components at year 10 of the 0.2° × 0.4° HBAY simulation. Vectors at every second grid point are plotted for clarity with the vector in southern Greenland providing the scaling. See the text for details. (bottom) Magnitude of the freshwater transport by (left) mean and (right) transient components. Note that the color and vector scales differ between the panels.

Sea deep convection in these models and its close proximity to the freshwater forcing, we focus our analysis here on the GIN Seas. Note that Hillaire-Marcel et al. (2001) argue that deep convection was absent in the Labrador Sea prior to the 8.2-kyr event.

Figure 13 (left) shows the freshwater content anomaly within the GIN convection region of the models. Note that it is difficult for tracers to enter or exit Hudson Bay at coarse resolution because of the limited number of grid points across the opening. In particular, in the 1.8° × 3.6° HBAY simulation the total salt content within Hudson Bay 50 years after forcing remains reduced by 40% relative to the control state, while in the 0.2° × 0.4° HBAY simulation the total salt content within Hudson Bay 50 years after forcing is only 5% lower than the control state. As a result the GIN freshwater content anomaly remains low throughout the 1.8° × 3.6° HBAY simulation, while for the 1.8° × 3.6° LC simulation the freshwater content quickly peaks and is flushed out of the primary convection region. In contrast, the longer-term entrainment of freshwater within Hudson Bay and along the continental shelf of the Labrador coast in the high-resolution simulations leads to a more consistent freshwater influence in the primary convection region, although as expected, the LC forcing anomaly is initially larger.

Changes in deep convection induced by the freshwater forcing are evaluated by considering grid cells that have 5-yr mean ventilation depths >100 m. In the both models the spatial pattern of convection determined from grid cells with 5-yr mean ventilation depths > 100 m was found to closely resemble the pattern of winter season (January–March) deep (>300 m) convection. Figure 13 (right) shows that the deep convection anomalies within the GIN Seas region are consistent with the surface freshwater content anomalies trends (Fig. 13, left).

4. Summary and conclusions

Using coarse (1.8° × 3.6°) and ocean eddy-permitting (0.2° × 0.4°) versions of a global climate model, we analyze the North Atlantic climate impacts of the 8.2-kyr

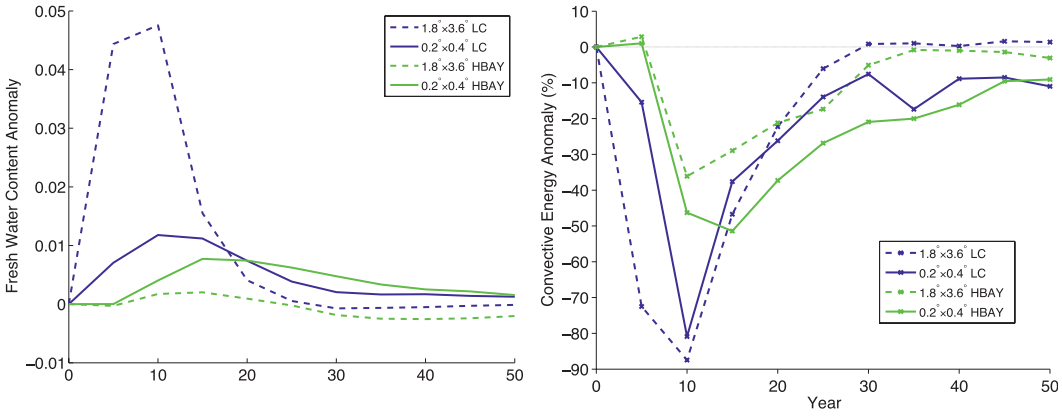

FIG. 13. (left) Freshwater content (i.e., $q = 1 - S/S_R$, where S is the near-surface salinity and $S_R = 34.9$ g kg^{-1} is a reference salinity) anomaly area weighted over the GIN Seas region (defined as 50°–80°N, 45°W–25°E). (right) Percentage change in deep convection in the GIN Seas region. All values are determined from 5-yr means. The deep convection analysis is limited to grid cells with 5-yr mean ventilation depths >100 m, which in the control state is found to closely resemble the spatial pattern of winter season deep (>300 m) convection.

event freshwater forcing. A large-scale cooling response and subsequent recovery path is found in all simulations regardless of the resolution or location of freshwater discharge. However, the magnitude and duration of the North Atlantic climate response is highly sensitive to model resolution and the location of freshwater forcing. Two sensitivities are consistently identified in the North Atlantic climate response. Firstly, irrespective of model resolution, the amount of entrainment and leakage of low-salinity water from Hudson Bay plays a key role in determining the duration of the climate response. In particular, discharging freshwater into Hudson Bay initially produces a weaker response relative to a Labrador Current freshwater discharge scenario, but a larger response on time scales beyond roughly 15 years. This sensitivity can be simply attributed to the longer time scale required for the low-salinity water to escape Hudson Bay. Second, the maximum decline in the AMOC and MHT is amplified by a factor of 2 at high resolution and the recovery time scale is increased by several decades, irrespective of the forcing region. The stronger and longer-term climate response at high resolution is partially attributed to the longer term entrainment of freshwater along the western boundary and its gradual, partially eddy-driven escape into the interior. Consequently, low-salinity anomalies in the North Atlantic deep convection regions persist for at least 50 years, which is nearly two decades longer than that found at coarse resolution.

A decomposition of ocean MHT reveals that the components driving the net MHT response are different at coarse and high resolution. At 1.8° × 3.6° the time-mean overturning component dominates the North Atlantic MHT response. At 0.2° × 0.4° the gyre mean component provides a substantial contribution to the net MHT decline poleward of 45°N, and significant transient overturning and gyre component anomalies are found equatorward of 25°N. The increased role of the gyre mean MHT component is attributed to a different linear vorticity balance response to the freshwater forcing at higher resolution. In particular, the enhanced role of bottom pressure torque in the linear vorticity balance at high resolution leads to a larger barotropic circulation response. The large horizontal viscosity required at coarse resolution severely limits the role of bottom pressure torque, and there is little change in the barotropic circulation at coarse resolution.

A significant caveat to the results presented here is that the simulations discussed here employ a time-invariant wind stress field. Indeed, the large barotropic circulation anomaly found at high resolution might be expected to induce a feedback response in models with a dynamic atmospheric component via modified surface buoyancy fluxes, which in turn could alter the position of winds and storm tracks. However, this feedback process is likely to be limited at coarse model resolutions because of the high ocean viscosity required by these models for numerical stability. Other coarse-resolution modeling studies have shown that the climate response in the subpolar Atlantic can strongly depend on a dynamic wind response (e.g., Saenko et al. 2007; LeGrande and Schmidt 2008; Clarke et al. 2009).

A recent high-resolution study of freshwater released into Hudson Bay suggested a weak impact on open ocean salinity and convection over the 10-yr period after forcing (Condron and Winsor 2011). Here we confirm this result, finding an initially weak Atlantic meridional overturning, meridional heat transport, surface air temperature,

and sea ice response in the North Atlantic when an 8.2-kyr event freshwater perturbation is applied to Hudson Bay at high resolution. However, we show that the advection of freshwater from Hudson Bay into the interior North Atlantic occurs over decades, and that this produces a strong and persistent long-term climate response in the high-resolution simulations presented here. These results could have important implications for studies of paleoclimate and future climate change in relation to freshwater perturbations in the North Atlantic. We note that a recent study by Weijer et al. (2012) finds a more persistent AMOC decline in a strongly eddying ocean model, relative to a coarser version, in response to present-day melt rates of the Greenland Ice Sheet.

Acknowledgments. This study was supported by the Australian Research Council, including the Centre of Excellence for Climate System Science. We are grateful for helpful discussions with Andrew Weaver and the computing support of the University of Victoria Climate Lab. We also thank the anonymous reviewers for their insightful comments.

REFERENCES

Alley, R., and A. Agustsdottir, 2005: The 8k event: Cause and consequences of a major Holocene abrupt climate change. *Quat. Sci. Rev.,* **24,** 1123–1149.

Barber, D., and Coauthors, 1999: Forcing of the cold event of 8,200 years ago by catastrophic drainage of Laurentide lakes. *Nature,* **400,** 344–348.

Bauer, E., A. Ganopolski, and M. Montoya, 2004: Simulation of the cold climate event 8200 years ago by meltwater outburst from Lake Agassiz. *Paleoceanography,* **19,** PA3014, doi:10.1029/2004PA001030.

Bond, G., W. Broecker, S. Johnsen, J. McManus, L. Labeyrie, J. Jouzel, and G. Bonani, 1993: Correlations between climate records from North Atlantic sediments and Greenland ice. *Nature,* **365,** 143–147.

Bryan, F., and R. Smith, 1998: Modelling the North Atlantic circulation: From eddy-resolving to eddy-permitting. *International WOCE Newsletter,* No. 33, WOCE International Project Office, Southampton, United Kingdom, 12–14.

Bryan, K., 1982: Poleward heat transport in the ocean: Observations and models. *Annu. Rev. Earth Planet. Sci.,* **10,** 15–38.

——, and L. Lewis, 1979: A water mass model of the World Ocean. *J. Geophys. Res.,* **84,** 2503–2517.

Chelton, D., R. deSzoeke, M. Schlax, K. Naggar, and N. Siwertz, 1998: Geographical variability of the first baroclinic Rossby radius of deformation. *J. Phys. Oceanogr.,* **28,** 433–460.

Clarke, G., D. L. J. Teller, and A. Dyke, 2004: Paleohydraulics of the last outburst flood from glacial Lake Agassiz and the 8200 BP cold event. *Quat. Sci. Rev.,* **23,** 389–407.

——, A. Bush, and J. Bush, 2009: Freshwater discharge, sediment transport, and modeled climate impacts of the final drainage of glacial Lake Agassiz. *J. Climate,* **22,** 2161–2180.

Condron, A., and P. Winsor, 2011: A subtropical fate awaited freshwater discharged from Lake Agassiz. *Geophys. Res. Lett.,* **38,** L03705, doi:10.1029/2010GL046011.

Ducet, N., P. Y. Le Traon, and G. Reverdin, 2000: Global high-resolution mapping of ocean circulation from TOPEX/Poseidon and ERS-1 and -2. *J. Geophys. Res.,* **105,** 19 477–19 498.

Fanning, A. F., and A. J. Weaver, 1997: A horizontal resolution and parameter sensitivity study of heat transport in an idealized coupled climate model. *J. Climate,* **10,** 2469–2478.

Flatau, M., L. Talley, and P. Niiler, 2003: The North Atlantic Oscillation, surface current velocities, and SST changes in the subpolar North Atlantic. *J. Climate,* **16,** 2355–2369.

Ganachaud, A., and C. Wunsch, 2000: Improved estimates of global ocean circulation, heat transport and mixing from hydrographic data. *Nature,* **408,** 453–457.

——, and ——, 2003: Large-scale ocean heat and freshwater transports during the World Ocean Circulation Experiment. *J. Climate,* **16,** 696–705.

Gent, P., and J. McWilliams, 1990: Isopycnal mixing in ocean circulation models. *J. Phys. Oceanogr.,* **20,** 150–155.

Griffies, S., and Coauthors, 2005: Formulation of an ocean model for global climate studies. *Ocean Sci.,* **1,** 45–75.

Hillaire-Marcel, C., C. de Vernal, G. Bilodeau, and A. Weaver, 2001: Absence of deep-water formation in the Labrador Sea during the last interglacial period. *Nature,* **410,** 1073–1077.

Johns, W., J. Bane, and D. Watts, 1995: Gulf Stream structure, transport, and recirculation near 68°W. *J. Geophys. Res.,* **100** (C1), 817–838.

Kistler, R., and Coauthors, 2001: The NCEP–NCAR 50-Year Reanalysis: Monthly means CD-ROM and documentation. *Bull. Amer. Meteor. Soc.,* **82,** 247–267.

Lazier, J., and D. Wright, 1993: Annual velocity variations in the Labrador Current. *J. Phys. Oceanogr.,* **23,** 659–678.

LeGrande, A., and G. Schmidt, 2008: Ensemble, water isotope–enabled, coupled general circulation modeling insights into the 8.2 ka event. *Paleoceanography,* **23,** PA3207, doi:10.1029/2008PA001610.

——, ——, D. Shindell, C. Field, R. Miller, D. Koch, G. Faluvegi, and G. Hoffman, 2006: Consistent simulations of multiple proxy responses to an abrupt climate change event. *Proc. Natl. Acad. Sci. USA,* **103,** 837–842.

Licciardi, J., J. Teller, and P. Clark, 1999: Freshwater routing by the Laurentide Ice Sheet during the last deglaciation. *Mechanisms of Global Climate Change at Millenial Time Scales, Geophys. Monogr.,* Vol. 112, Amer. Geophys. Union, 177–201.

Lozier, M., 2010: Deconstructing the conveyor belt. *Science,* **328,** 1507–1511.

McAvaney, B., and Coauthors, 2001: Model evaluation. *Climate Change 2001: The Scientific Basis,* Cambridge University Press, 471–523.

Meissner, K., and P. Clark, 2006: Impact of floods versus routing events on the thermohaline circulation. *Geophys. Res. Lett.,* **33,** L15704, doi:10.1029/2006GL026705.

Oschlies, A., 2002: Improved representation of upper-ocean dynamics and mixed layer depths in a model of the North Atlantic on switching from eddy-permitting to eddy-resolving grid resolution. *J. Phys. Oceanogr.,* **32,** 2277–2298.

Pacanowski, R., 1996: MOM 2 documentation user's guide and reference manual. GFDL Ocean Group Tech. Rep. 3.2, NOAA/GFDL, 329 pp.

Rahmstorf, S., 2002: Ocean circulation and climate during the past 120,000 years. *Nature,* **419,** 207–214.

Randall, D., and Coauthors, 2007: Climate models and their evaluation. *Climate Change 2007: The Physical Science Basis.* Cambridge University Press, 589–662.

Renssen, H., H. Goosse, and T. Fichefet, 2002: Modeling the effect of freshwater pulses on the early Holocene climate: The influence of high frequency climate variability. *Paleoceanography,* **17,** 1020, doi:10.1029/2001PA000649.

Rohling, E., and H. Palike, 2005: Centennial-scale climate cooling with a sudden cold event around 8,200 years ago. *Nature,* **434,** 975–979.

Saenko, O., 2009: On the climatic impact of wind stress. *J. Phys. Oceanogr.,* **39,** 89–106.

——, A. Weaver, D. Robitaille, and G. Flato, 2007: Warming of the subpolar Atlantic triggered by freshwater discharge at the continental boundary. *Geophys. Res. Lett.,* **34,** L15604, doi:10.1029/2007GL030674.

Smethie, W., R. Fine, A. Putzka, and E. Jones, 2000: Tracing the flow of North Atlantic Deep Water using chlorofluorocarbons. *J. Geophys. Res.,* **105** (C6), 14 297–14 324.

Smith, R., M. Maltrud, F. Bryan, and M. Hecht, 2000: Numerical simulation of the North Atlantic at 1/10°. *J. Phys. Oceanogr.,* **30,** 1532–1561.

Spence, P., M. Eby, and A. Weaver, 2008: The sensitivity of the Atlantic meridional overturning circulation to freshwater forcing at eddy-permitting resolutions. *J. Climate,* **21,** 2697–2710.

——, O. Saenko, W. Sijp, and M. England, 2012: The role of bottom pressure torques on the interior pathways of North Atlantic Deep Water. *J. Phys. Oceanogr.,* **42,** 110–125.

Stammer, D., 1997: Global characteristics of ocean variability estimated from regional TOPEX/POSEIDON altimeter measurements. *J. Phys. Oceanogr.,* **28,** 1743–1769.

Stommel, H., 1961: Thermohaline convection with two stable regimes of flow. *Tellus,* **13,** 224–230.

Stouffer, R., and Coauthors, 2006: Investigating the causes of the response of the thermohaline circulation to past and future climate changes. *J. Climate,* **19,** 1365–1387.

Talley, L., 2003: Shallow, intermediate, and deep overturning components of the global heat budget. *J. Phys. Oceanogr.,* **33,** 530–560.

Teller, J., D. Leverington, and J. Mann, 2002: Freshwater outbursts to the ocean from Lake Agassiz and their role in climate change during the last deglaciation. *Quat. Sci. Rev.,* **21,** 879–887.

Treguier, A., S. Theetten, E. Chassignet, T. Penduff, R. Smith, L. Talley, J. Beismann, and C. Böning, 2005: The North Atlantic subpolar gyre in four high-resolution models. *J. Phys. Oceanogr.,* **14,** 757–774.

Trenberth, K. E., and J. Caron, 2001: Estimates of meridional atmosphere and ocean heat transports. *J. Climate,* **14,** 3433–3443.

Volkov, D., L.-L. Fu, and T. Lee, 2010: Mechanism of the meridional heat transport in the Southern Ocean. *Ocean Dyn.,* **60,** 791–801.

Weaver, A. J., and Coauthors, 2001: The UVic Earth System Climate Model: Model description, climatology, and applications to past, present and future climates. *Atmos.–Ocean,* **39,** 361–428.

Weijer, W., M. Maltrud, M. Hecht, H. Dijkstra, and M. Kliphuis, 2012: Response of the Atlantic Ocean circulation to Greenland Ice Sheet melting in a strongly-eddying ocean model. *Geophys. Res. Lett.,* **39,** L09606, doi:10.1029/2012GL051611.

Willebrand, J., B. Barnier, C. Böning, C. Dieterich, P. Killworth, C. L. Provost, Y. Jia, J. Molines, and A. New, 2001: Circulation characteristics in three eddy permitting models of the North Atlantic. *Prog. Oceanogr.,* **48,** 123–161.

Wunsch, C., 1999: Where do ocean eddy heat fluxes matter? *J. Geophys. Res.,* **104** (C6), 13 235–13 249.

——, 2007: The past and future ocean circulation from a contemporary perspective. *Ocean Circulation: Mechanisms and Impacts—Past and Future Changes of Meridional Overturning, Geophys. Monogr.,* Vol. 173, Amer. Geophys. Union, 53–74.